ISBN: 978-3-95450-211-0 doi:10.18429/JACoW-SRF2019-THP036

AN INSIGHT ON THE THERMAL AND MECHANICAL NUMERICAL EVALUATIONS FOR THE HIGH-LUMINOSITY LHC CRAB CAVITIES*

E. Cano-Pleite†, A. Amorim, K. Artoos, R. Calaga, O. Capatina, T. Capelli, F. Carra, L. Dassa, M. Garlasché, R. Leuxe, E. Montesinos, CERN, Geneva, Switzerland
J. A. Mitchell, Lancaster University, Lancaster, UK
S. Verdú-Andrés, Brookhaven National Laboratory, Upton, NY, USA

Abstract

One of the key devices of the HL-LHC project are SRF crab cavities. A cryomodule with two Double Quarter Wave (DQW) crab cavities has been successfully fabricated and tested with beam at CERN whereas the Radio Frequency Dipole (RFD) crab cavities are currently on its fabrication process. The paper provides an insight on the multiple calculations carried out to evaluate the thermal and mechanical performance of the DQW and RFD cavities and its components. In some cases, the presence of RF fields inside the cavity volume requires the use of multiphysics numerical models capable of coupling these fields with the thermal and mechanical domains. In fact, the RF field presents a strong dependency on the cavity shape, whereas the mechanical, thermal and electrical properties of the materials may substantially vary as a function of temperature, which in turn depends on the RF field. The results presented in this paper, using both coupled and uncoupled models, allowed elucidating the importance of physics coupling on the numerical evaluation of RF cavities and its components. Analyses were also of great support for the design evaluation and improvement of future prototypes.

INTRODUCTION

Superconducting Radio Frequency (SRF) crab cavities are key components of the High Luminosity LHC upgrade (HL-LHC). The electromagnetic field inside of the cavities provides a deflecting kick on the proton beam, tilting the particle bunches and thus maximizing their overlap at the interaction points [1]. Two designs are used for HL-LHC: the Double Quarter Wave (DQW) [2] and the Radio Frequency Dipole (RFD) [3] (see Fig. 1). During 2018, a cryomodule with two DQW crab cavities was successfully tested with beam at CERN in the SPS whereas the RFD crab cavities are currently under fabrication [4].

The cavities are placed in a cryomodule and are cooled down to 2 K with superfluid helium. The static and dynamic heat losses of the cryomodule were evaluated in previous works [5, 6]. To limit the heat loss of the cavity ancillaries due to the RF heating in dynamic conditions, some of their parts are made out of high purity niobium (Nb) that becomes superconducting at cryogenic temperatures. For such temperatures, the material properties, both electrical and thermal, are non-linear and highly dependent on temperature itself.

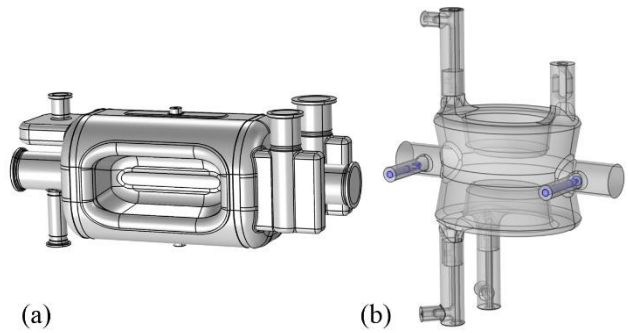

Figure 1: 3D models of the (a) RFD cavity for structural evaluations and (b) DQW cavity with antennas for thermal evaluations.

The cavities are equipped with a tuning system that ensures the operation of the cavity at the required frequency [7]. The cavity frequency may deviate from its nominal value due to permanent deformations induced by pressure tests done during the cavity lifespan. In addition, pressure fluctuations of the He bath and the radiation pressure generated by the electromagnetic field can elastically change the shape of the cavity, modifying its frequency during operation. To this end, Pressure Sensitivity (PS) and Lorentz Force Detuning (LFD) are two paramount parameters in the performance of RF cavities.

The aim of the present paper is to provide an insight on the multiple numerical evaluations - mechanical, thermal and electromagnetic - used for the design improvement and optimization in the context of the crab cavity project. In some cases, the thermal and mechanical performances of the cavities and subcomponents shall consider the presence of electromagnetic fields inside the cavity, and thus require an adequate physics coupling. In addition to valuable numerical information, the results here presented provide an insight on the capabilities of multiphysics modelling on the numerical assessment of such cavities.

GENERAL APPROACH

This part is divided in two sections. The first one describes the parameters used to analyse the cavities mechanical behaviour. The second section discusses the procedure followed for the electromagnetic-thermal coupled evaluation of the cavity RF antennas. The same division is also followed in the results section.

* Work supported by by the HL-LHC project.
† eduardo.cano.pleite@cern.ch

ISBN: 978-3-95450-211-0 doi:10.18429/JACoW-SRF2019-THP036

Mechanical Evaluation

Cavity tunability Both the DQW and the RFD crab cavities have a nominal operating frequency of 400.79 MHz. The cavities are equipped with a tuning system (and a pre-tuner in the case of DQW) to ensure this value regardless of the multiple effects affecting the cavity shape during their manufacturing and testing [7]. The tuner locally deforms the cavity walls in the elastic domain, promoting a variation of its fundamental frequency. In the case of DQW cavity, the tuner also provides stiffening in the cavity sensitive region: the capacitive plates. The tunability (in kHz/mm) measures the ability to change the cavity frequency as a function of the deformation applied on its walls.

Pressure sensitivity and pressure test Fluctuations on the pressure of the superfluid helium bath cause a detuning of the cavity due to small elastic changes on its shape. Pressure sensitivity measures the frequency shift attributed to these slow pressure fluctuations, which are typically of the order of mbar.

Additionally, the cavities shall be pressure tested according to the appropriate standards [8]. The pressure test is generally at a higher pressure than the cavity service pressure and may promote a permanent deformation on the cavity body that produces changes on its fundamental frequency. The use of coupled RF-structural calculations allows the prediction of this frequency shift and the application of correcting actions to minimize this effect.

Lorentz force detuning The RF fields in the cavity volume produce a radiation pressure on the cavity walls that is proportional to the square of the magnetic, H, and electric, E, fields [9, 10]:

$$P_{LFD} = \frac{1}{4}(\mu_0 H^2 - \varepsilon_0 E^2) \qquad (1)$$

The deformation induced by the radiation pressure when the cavity is operated in CW mode produces a shift on the fundamental frequency of the cavity.

The design of the cavity shall be focused on minimizing PS and LFD while guaranteeing a locally flexible (i.e. tunable) cavity. Therefore, all these parameters shall be carefully accounted for during the cavity design stage.

Thermal Evaluation

The electromagnetic fields in the cavity generate currents in the cavity antennas that dissipate heat by Joule effect. The power dissipated depends on the surface resistance (R_s) and the magnetic field intensity at the surface of the conductor (H):

$$\frac{dP}{dA} = \frac{1}{2} R_s |\hat{\boldsymbol{n}} \times \boldsymbol{H}|^2 \qquad \text{with} \qquad R_s = \sqrt{\frac{\mu\omega}{2\sigma}} \qquad (2)$$

Note that, in Eq. (2), the power dissipated in the antenna depends on the surface resistance, which in turn varies with temperature, as it depends on the electrical conductivity of the material (σ). Hence, for an adequate evaluation of the heat loss in the antennas, it is necessary to couple the RF and thermal physics in order to account for both thermal and electrical properties that depend on temperature.

NUMERICAL MODELING

Figure 1 shows 3D models used for the evaluation of the DQW and RFD bare cavities. The mechanical response to the pressure test, the pressure sensitivity and Lorentz force detuning were calculated using the numerical model of the RFD cavity shown in Fig. 1(a). This model is a simplification of the model used for the thermal evaluation of the RFD cavity that only contains its antennas and the vacuum volume. Thermal analyses on the DQW antennae were performed using the model in Fig. 1(b). Note that all the analyses coupled the RF domain with the mechanical or thermal domains. Therefore, the models shall consider both the vacuum (for RF calculations) and the solid (for structural and thermal calculations) domains.

Materials

The mechanical properties in Table 1 were used for the structural analyses of the cavities at cryogenic (PS and LFD) and room temperatures (pressure test). In particular, for the DQW tunability analysis, properties similar to those of previous analyses [11] were used for the sake of comparison. For the pressure test numerical evaluations, elasto-plastic material models with $R_{p0.2}$ of 65 MPa were used.

Table 1: Mechanical Properties Used for Nb [12, 13]

Density [kg/m^3]	Poisson's ratio [-]	Young's modulus (2 K) [GPa]	Young's modulus (Room) [GPa]
8600	0.38	118	106

The RF antennas here analysed are made of copper (Cu) and/or high purity niobium (RRR300). In the case of copper the surface resistance increases by 20-30 % due to the anomalous skin effect [14]. For superconducting niobium the surface resistance has two adding terms: the BCS and the residual resistance.

Two different approaches were followed for the thermal evaluations: a first estimation with thermally independent properties and a second approach using temperature-dependent thermal and electrical conductivities [15, 16]. For the former, the temperature dependence of the surface resistance of Nb is considered by using a residual resistance of 20 nΩ and temperature-dependent BCS resistance. In the case of copper, the surface resistance of Cu RRR90 was scaled up accounting for the anomalous skin effect considering a surface resistance of 1 mΩ at 2 K.

Simulation Procedure and boundary Conditions

The simulation methodology for the structural evaluation of the RFD cavity is similar in all the cases.

Firstly, an eigenfrequency problem is solved to obtain the fundamental frequency of the cavity, f_0. Secondly, the structural problem is solved, which is coupled with the deformation of the mesh in the vacuum volume. The structural calculations assume the cavities fixed in all the

ISBN: 978-3-95450-211-0 doi:10.18429/JACoW-SRF2019-THP036

flanges except the pick-ups, emulating the cavity inserted in an infinitely stiff He vessel. The presence of the tuning system was modelled by a spring of stiffness k_s between the tuning surfaces for the PS and LFD evaluations. Lastly, the fundamental frequency of the deformed cavity volume is calculated, f_1. The values of the tunability, PS and LFD can be then obtained relating the frequency shift with the tuning displacement, $|v_t|$, the pressure, P_{PS}, and the square of the field, V_T, respectively, as depicted in Table 2.

Table 2: Equations to Calculate Tunability, PS and LFD

Tunability [kHz/mm]	PS [Hz/mbar]	LFD [Hz/MV²]
$\frac{f_1 - f_0}{\lvert v_t \rvert}$	$\frac{f_1 - f_0}{P_{PS}}$	$\frac{f_1 - f_0}{{V_T}^2}$

In general, commercial software scale the fields to some value of the energy stored in the cavity. In the particular case of LFD and the thermal calculations, it is necessary to scale up the fields to the nominal deflecting kick on the particle bunch. To do so, the deflecting kick in the axis of the cavity was integrated following Eq. (3) and scaled up to match the expected deflecting voltage of the cavity.

$$V_T = \left| \int E_y \cos\left(\frac{\omega x}{c}\right) dx + \int \mu_0 c \cdot H_z \sin\left(\frac{\omega x}{c}\right) dx \right| \quad (3)$$

Where x represents the coordinate of the particle bunch along the beam direction; E_y and H_z represent the main components of the electric and magnetic field at the cavity axis, respectively; c is the speed of light; ω is the angular frequency and μ_0 is the vacuum permeability.

RESULTS

Mechanical Evaluations

Tunability – DQW cavity Figure 2 shows the deformation of the DQW cavity body when a pulling displacement of 1 mm is applied to its top and bottom plates. The frequency shift of the cavity after this deformation results in 315.5 kHz/mm. This result, obtained with COMSOL Multiphysics, is consistent with the 318 kHz/mm encountered in previous works for the same numerical conditions and a different software [11].

The calculated value of the cavity tunability was compared against experimental results obtained during the testing of the DQW cavities at CERN SM18 in 2018.

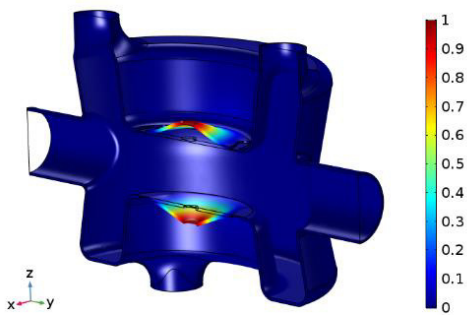

Figure 2: Contour plot of the displacement (in mm) in the DQW cavity. Tuner pulling displacement of 1 mm.

Figure 3 shows a comparison of the experimental and numerical results of the frequency shift of the cavity as a function of the force applied by the tuner. The similarity between the numerical predictions and the experimental results is remarkable. The difference between them increases progressively with the applied force due to the slight different slope of the curves. It is worth to mention that Fig. 3 implicitly includes the transformation from displacement to force in the ensemble of the tuning system, which introduces an incertitude in the comparison between experimental and numerical results. Despite of this, the certainty, the simplicity and the closeness between the numerical and the experimental results confirm the application of this coupling strategy for an adequate prediction of the cavity tunability.

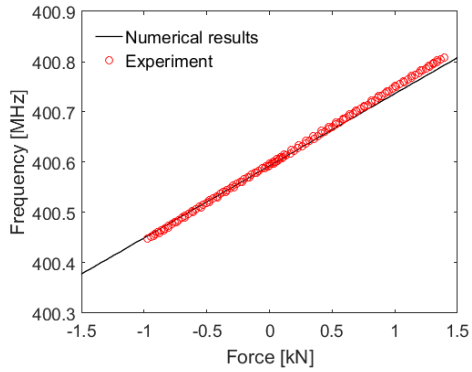

Figure 3: Frequency of the DQW cavity as a function of the force generated by the tuner system. Numerical results are derived from COMSOL and the tuning system stiffness.

Pressure sensitivity – RFD cavity Figure 4 shows the unscaled electric and magnetic fields of the RFD cavity volume at the fundamental frequency and the magnetic field for an aimed total stored energy in the cavity of 10.7 J, which corresponds to a deflecting kick of 3.41 MV. Once the fundamental frequency was obtained, a pressure of 1 bar was applied to the external walls of the cavity, resulting on their deformation. The frequency in the deformed cavity was then recalculated to evaluate the pressure sensitivity of the cavity, resulting in -193 Hz/mbar.

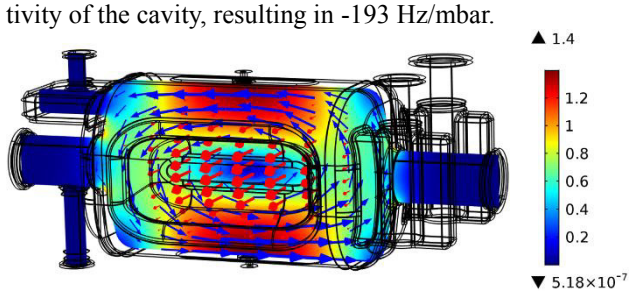

Figure 4: Qualitative vectors of the electric (red) and magnetic (blue) fields combined with contours of the magnetic field (in A/m) in a central slice of the cavity vacuum volume. Deflecting kick of 3.41 MV.

Lorentz force detuning – RFD cavity Figure 5 shows the deformation due to radiation pressure on the cavity walls resorting from a deflecting kick of 3.41 MV. The magnetic repulsive forces tend to push the cavity top and

ISBN: 978-3-95450-211-0 doi:10.18429/JACoW-SRF2019-THP036

bottom plates to the exterior of the cavity, promoting a decrease of the cavity fundamental frequency, whereas the electric forces tend to join the poles together, which also promotes a decrease of the cavity frequency. The value obtained for the Lorentz force detuning after recalculating the frequency in the deformed model is - 555 Hz/MV^2.

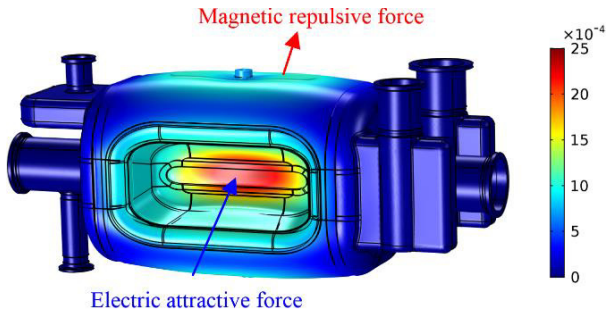

Figure 5: Displacement of the cavity walls (in mm) due to the radiation pressure. Deflecting kick of 3.41 MV.

A precise evaluation of the Lorentz Force detuning requires the use of a fully coupled RF-structural calculation: the electromagnetic field induces a change in the shape of the cavity that modifies the electromagnetic field, which affects the radiation pressure applied to the cavity walls. This mutually interacting behaviour was numerically evaluated and lead to negligible variations in the value of LFD.

The results presented above can provide valuable information on the optimal stiffness of the tuning system, k_s. Figure 6 shows the variation of the absolute value of PS and LFD with k_s and reveals opposed trends of the tuner stiffness on PS and LFD. This behaviour can be easily explained by the counteracting effect that the pressure-induced deformation of the pole (negative frequency shift) and the tuning regions (positive frequency shift) have on the fundamental frequency of the cavity.

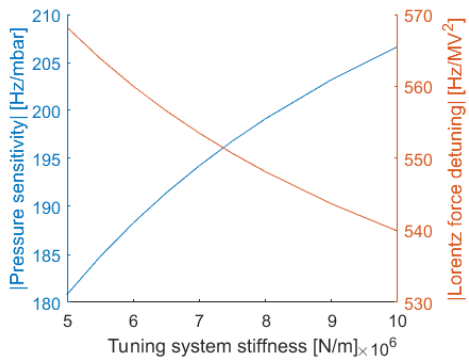

Figure 6: Evolution of the absolute value of the PS and LFD as a function of the tuning system stiffness.

Pressure tests – DQW and RFD cavities Pressure test calculations were also performed to provide a first estimation of the permanent frequency shift of the cavities during their testing campaign. For that, elasto-plastic simulations with a yield strength of Nb of 65 MPa were performed on both cavity models and using a stress-strain curve measured at CERN [17]. The results are shown in Table 3, which also includes values of the frequency shift using an elastic-perfectly plastic material model, and reveal relatively small differences between both approaches (around 12 %). A benchmark of these calculations using the experimental results of the frequency shift of the DQW cavity prototypes during their testing is currently ongoing.

Table 3: Pressure Test Frequency Shift Simulations

Material model	RFD	DQW
Elastic-perfectly plastic	20.7 kHz	-15.8 kHz
Realistic	18.3 kHz	-14.2 kHz

Thermal Evaluations

Thermally independent material properties As a first study, three different commercial software products were used for the thermal evaluation of the DQW "hook" copper antenna (Fig. 7). A direct visual comparison of the results obtained in COMSOL, CST and ANSYS-HFSS was done by simulating the field and temperature on the surface of the pickup antenna after solving an eigenfrequency problem using thermally-independent material properties. These calculations aimed for 1 J stored energy in the cavity, which corresponded to a deflecting kick of around 1.04 MV in the three cases. Due to the different internal algorithms used in the three programmes for the solution of the eigenvalue problem, the fields needed to be appropriately scaled for each case. It can be clearly appreciated in Fig. 7 that the maximum temperature in the antenna and its evolution with the kick voltage is perfectly matching for the three software products. The values fit to a quadratic function, as constant material properties are used. Figure 7 also shows the H field and the temperature distribution in the antenna. The maximum field takes place in the central part of the hook and the maximum temperature is located in the tip of the antenna in all cases.

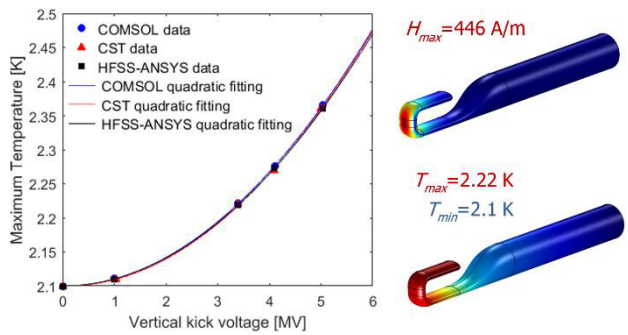

Figure 7: Maximum temperature in the pickup antenna as a function of the vertical kick. Copper properties at 2.1 K.

Thermally dependent material properties COMSOL was used for the subsequent analyses accounting for thermally dependent material properties due to its simplicity for the coupling of physics. The effect of using constant material properties is analysed in Fig. 8, which depicts the heat loss and maximum temperatures of the second pickup antenna of DQW cavity (viz. mushroom) if it were done in copper and using constant and thermally dependent material properties. Note that not accounting for the material dependence with temperature can create differences in the temperature increase up to a 25 % for a deflecting kick of

ISBN: 978-3-95450-211-0 doi:10.18429/JACoW-SRF2019-THP036

5 MV. In this particular case, the heat loss remains equal for both cases, as the copper electrical conductivity presents a negligible variation on the 4 to 15 K range. The use of this coupling strategy becomes critical when using superconducting materials [18], as inappropriately simulating thermal dependent properties may lead to misleading conclusions when trying to precisely predict thermal instabilities and quenches.

Figure 8 also shows the magnetic field distribution in the surface of the antenna, which presents a maximum value of 5000 A/m in the border of the mushroom. The temperature distribution for an antenna done in copper and 3.41 MV deflecting kick is also depicted in the figure. As in the case of the hook, the maximum temperature takes place in the tip of the antenna.

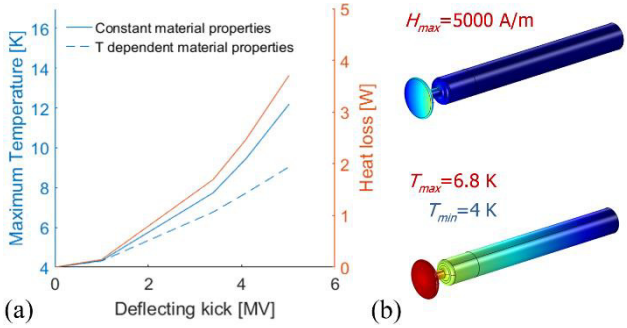

Figure 8: DQW mushroom antenna. (a) Maximum temperature and heat loss as a function of the deflecting kick. (b) H field and T distribution on the antenna.

To reduce the heat loss of this antenna, it was decided to use Nb on its tip, with a length that extends to the required distance to correctly weld the Cu and Nb interfaces (see the circumferential black line in Fig. 8). In this new situation, calculated using a fully coupled model, the maximum temperature increase is 4 mK and the heat loss is below 3 mW. Comparing this results with those in Fig. 8 one can note the dramatic decrease of both the maximum temperature and heat loss as compared to the Cu antenna.

The same exercise previously described was done for the thermal evaluation of the preliminary design of the pickup and V-HOM antennas of the RFD cavity. First, similarly to the abovementioned studies, the effect of introducing Nb in the tip of the V-HOM antenna was analysed. The results in Fig. 9 show the distribution of the temperature increase for different lengths of niobium. It is worth to note that the temperature increase is negligible as soon as niobium is introduced in the model. The heat loss also dramatically decreases by a factor of 130 in comparison with the antenna integrally done in Cu.

A similar study was carried out for the vertical pick-up antenna of the RFD cavity. As for DQW, the initial design of the antenna is made of copper. In this situation, the maximum temperature increase for a deflecting kick of 3.41 MV is 0.017 K with a heat loss of 3.4 mW. Both the temperature increase and the heat loss remain very low even if the deflecting kick is increased (see Fig. 10). Thus, the use of Nb in this antenna is initially discarded.

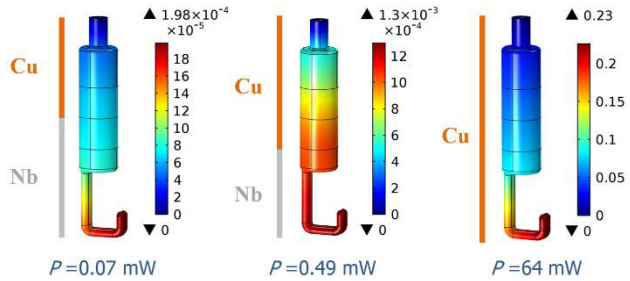

Figure 9: Temperature increase distribution (in K) and heat loss in the RFD V-HOM antenna for different length of niobium and a deflecting kick of 3.41 MV.

In an opposed way to the calculations previously done for the DQW pick-up antennas, the use of fully coupled models in calculations in which the temperature decrease is small, such as in the RFD pick-up antenna, can be considered unnecessary, as the change of the thermal properties of the material will be marginal.

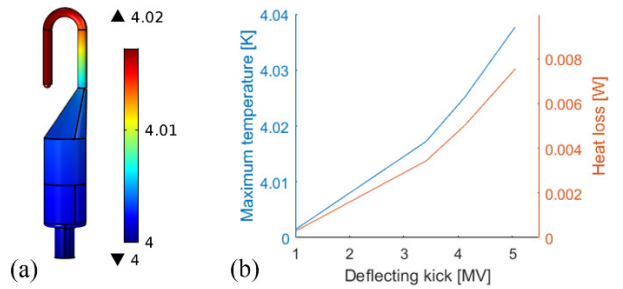

Figure 10: RFD pickup antenna. (a) Temperature distribution (in K) for a deflecting kick of 3.41 MV. (b) Maximum temperature and heat loss as a function of the deflecting kick.

CONCLUSIONS

This paper presented the general approach, the numerical procedure and valuable results on multiphysics calculations of some of the key parameters of the numerical assessment of the crab cavities of the HL-LHC upgrade. The assessments included the evaluation of the frequency variations due to mechanical actions on the cavities and the heat losses due to electromagnetic heating of the cavity ancillaries. The results, obtained for both DQW and RFD cavities, were of great use for the improvement of the cavities design and the correct determination of the materials of the cavity antennas. In addition, the analysis here presented highlight the importance of physics coupling on the evaluation of this type of cavities and their corresponding ancillaries.

ACKNOWLEDGEMENTS

The RF designs used in this contribution were provided by the HL-LHC-AUP collaboration. The authors are grateful for their continuous help and for all the fruitful discussions.

REFERENCES

[1] G. Apollinari, I. Béjar Alonso, O. Brüning, P. Fressia, M. Lamont, L. Rossi, L. Tavian, "High-Luminosity Large

ISBN: 978-3-95450-211-0 doi:10.18429/JACoW-SRF2019-THP036

Hadron Collider (HL-LHC) Technical Design Report v.0.1", *CERN Yellow Reports: Monographs 4 ISBN 9789290834717*, 2017.

[2] S. Verdú-Andrés *et al.*, "Design and vertical tests of double-quarter wave cavity prototypes for the high luminosity LHC crab cavity system", *Phys. Rev. Accel. Beams,* 21, 082002, 2018.

[3] S. U. De Silva and J. R. Delayen, "Design evolution and properties of superconducting parallel-bar rf-dipole deflecting and crabbing cavities", *Phys. Rev. Accel. Beams,* 16, 012004, 2013.

[4] R. Calaga *et al*., "Crab cavities: SPS test results, design advancement, plans for production", *8th HL-LHC Collaboration Meeting,* CERN, 2018. Site: https://indico.cern.ch/event/742082/contributions/3072164/

[5] F. Carra *et al.*, "Assessment of thermal loads in the CERN SPS crab cavities cryomodule", *J. Phys.: Conf. Ser.*, 874 012005, 2017.

[6] E. Cano Pleite *et. al.*, "Numerical and Experimental Evaluation of the DQW Crab Cavity Cryomodule Thermal Budget", in *Proc. IPAC '19*, Melbourne, Australia, 2019.

[7] K. Artoos *et al.*, "Status of the HL-LHC crab cavity tuner", in *Proc. SRF '19*, Dresden, Germany, 2019, this conference.

[8] Pressure Equipment Directive (PED) 2014/68/EU.

[9] S. Verdú-Andrés *et al.*, "Lorentz detuning for a double-quarter wave cavity", in *Proc. SRF '15*, Whistler, BC, Canada, 2015.

[10] R. Mitchell *et al.*, "Lorentz force detuning analysis of the spallation neutron source (SNS)", in the *10th workshop on RF Superconductivity*, Tsukuba, Japan, 2001.

[11] S. Verdú-Andrés, "Slides on 'ACE3P Calculation", BNL, 2016.

[12] M. Merio, "Material properties for engineering analyses of RF cavities", Fermilab, 2013.

[13] L. Dassa, "EDMS 1530740 – Crab cavity – Material properties for mechanical analysis", CERN, 2019.

[14] W. Chou and F. Ruggiero, "Anomalous skin effect and resistive wall heating", *LHC Project Note 2 (SL/AP)*, CERN, Geneva, Switzerland, 1995.

[15] Cryocomp, Eckels Engineering, 2011.

[16] H. Padamsee, "The science and technology of superconducting cavities for accelerators", Supercond. Sci. Technol. 14, R28-R51, 2001.

[17] A. Gerardin, "EDMS 1493400 – Tensile tests of Nb samples", CERN, 2015.

[18] S. Verdú-Andrés *et al.*, "Cryogenic RF performance of Double-Quarter Wave cavities equipped with HOM filters", in *Proc. IPAC '19*, Melbourne, Australia, 2019.